Michigan State University

National Superconducting Cyclotron Laboratory

ANOTHER LOOK AT "SOFT" LEPTON PAIR PRODUCTION IN NUCLEON-NUCLEON BREMSSTRAHLUNG

JIANMING ZHANG, RAHMA TABTI, CHARLES GALE, and KEVIN HAGLIN

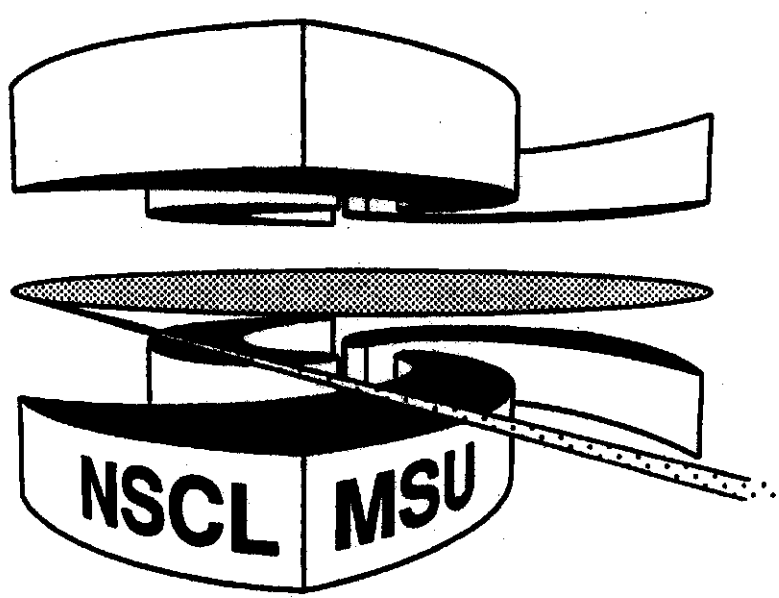

MSUCL-961 **JUNE 1995**

McGill/94-56

MSUCL-961

Another look at "soft" lepton pair production in nucleon-nucleon bremsstrahlung

Jianming Zhang*, Rahma Tabti†, and Charles Gale*

Physics Department, McGill University, Montréal, Québec, Canada *H3A-2T8*

Kevin Haglin§

National Superconducting *Cyclotron Laboratory,* Michigan State University

East Lansing, MI 48824-1321 USA

Abstract

We compare different formalisms for the calculation of lepton pair emission in hadron-hadron collisions and discuss the consequences of the approximations inherent to each of them. Using a Lorentz-covariant and gauge-invariant formalism proposed by Lichard, we calculate lepton pair emission via bremsstrahlung in proton-proton and neutron-proton reactions at energies between 1 and 5 GeV to leading order in the virtual photon four-momentum. These new results suggest that some previous bremsstrahlung calculations based on varieties of the soft-photon approximation might have somewhat

"Electronic address: jzhang@hep.physics.mcgill.ca

†Electronic address: tabti@hep.physics.mcgill.ca

*Electronic address: gale@hendrix.physics.mcgill.ca

§Electronic address: haglin@theo03.nscl.msu.edu

overestimated the DLS low-mass dilepton cross sections. We find that the respective intensities of dilepton production through pp and np bremsstrahlung are energy-dependent and become comparable at $E_{\rm kin} \gtrsim 2$ GeV. We also calculate the polar angle anisotropy of the lepton spectrum.

I. INTRODUCTION

Dileptons and photons are probably the best carriers of information from the hot and compressed nuclear matter produced in the early stages of heavy-ion collisions [1]. In principle, those electromagnetically interacting particles can leave the hadronic environment from which they are created without significant disturbances, offering a relatively clean probe of the nuclear collision dynamics. In heavy ion collisions at incident energies of 1–5 A GeV, where the Lawrence Berkeley Laboratory Dilepton Spectrometer (DLS) has already taken measurements [2], the most important sources of e^+e^- pairs seem to be Dalitz and radiative decays—mainly from η mesons and Δ's, pion-pion annihilations, and nucleon-nucleon bremsstrahlung [3–5]. Measurements of lepton pair production in single nucleon-nucleon reactions have also recently been performed in the GeV energy regime. In those, the measured pd/pp dielectron yield ratios display a clear beam energy as well as invariant mass dependence [6]. This suggests that the dominant mechanism for dilepton production may be changing as the beam energy per nucleon increases from 1 to 5 GeV. In particular, one should pay attention to the opening of inelastic nucleon-nucleon channels. The latter have been shown to play an important role for dielectron production in nucleon-nucleon collisions at 4.9 GeV [5]. To eventually understand quantitatively and completely the relative role of all these contributions and their excitation function in the complex environment of nucleus-nucleus collisions, it is vital to first calculate the lepton pair production cross sections for individual processes as accurately as possible. Here we shall concentrate on the bremsstrahlung generation of lepton pairs in the case of nucleon-nucleon reactions.

Several different calculations for electron-positron pair emission through nucleon-nucleon bremsstrahlung have been performed for reactions at, and slightly above, 1 GeV. Some of the more sophisticated approaches used relativistic one-boson exchange (OBE) Lagrangians, with the coupling to the electromagnetic field done by minimal substitution [7–9]. These approaches are thus entirely Lorentz-covariant and are also gauge-invariant in the electromagnetic sector. Note that the OBE dilepton calculations can be made gauge-invariant even

when form factors at the strong interactions vertices are used [7]. Such approaches have all the transformation properties that are required of a complete theory but they are not completely satisfactory in two respects. First, they are very cumbersome. If several meson fields are involved, the number of Feynman graphs to be evaluated proliferates rapidly and the difficulty of the calculations increases accordingly. The coupling constants in the OBE model are fitted such that the total nucleon-nucleon cross sections are reproduced as closely as possible. This exercise thus has to be repeated for each colliding system. Second, even if two different OBE calculations with two slightly different set of ingredients (meson fields, form factors and coupling constants) can do a good job of generating total nucleon-nucleon cross sections that are in agreement with experimental measurements, generally they will have different predictions for the differential cross sections. As we shall see below, there is a way of writing the low invariant mass dilepton production cross section in nucleon-nucleon collisions such that it clearly depends on the differential elastic cross section of the colliding partners. This fact thus imposes very stringent requirements on the OBE models as far as their ability to predict lepton pair production yields is concerned. This point was recently made in the literature [10,5]. Because of the above considerations, the calculations pertaining to the bremsstrahlung generation of low invariant mass lepton pairs in nucleon-nucleon collisions have used a "soft photon approximation" [11] of some kind or another. Almost all of the recent calculations of dielectron production in nucleon-nucleon (and nucleus-nucleus) collisions that have used the soft photon approximation have used as their starting point a formula suggested by Rückl [14]:

$$E_+E_-\frac{d^6\sigma^{e^+e^-}}{d^3p_+d^3p_-} = \frac{\alpha}{2\pi^2}\frac{1}{M^2}\left(\omega\frac{d^3\sigma^\gamma}{d^3q}\right)_{\vec{q}=\vec{p_+}+\vec{p_-}} . \qquad (1)$$

This equation links the cross section for production of dileptons via virtual photon bremsstrahlung to the bremsstrahlung cross section for real photons. In the above, $\vec{p_\pm}$ is the three-momentum of the electron or positron, $E_\pm$ is the energy, $M^2 = (p_+ + p_-)^2$ is the dilepton invariant mass squared, $\vec{q}$ is the photon momentum and ω is its energy. The fine structure constant appears as α.

The derivation of soft photon formulæ in the context of bremsstrahlung emission of lepton pairs has recently been re-analyzed [12]. It was shown that Rückl's formula was not properly Lorentz-covariant and did not contain the relationship between dilepton cross section and virtual photon cross section that is required by gauge invariance [15]. In the context of the new analysis of dilepton production via virtual photon bremsstrahlung, a new set of formulæ were derived for the leading order and next-to-leading order contributions to lepton pair emission [12].

It had been known for some time that the Rückl formula was not entirely correct [16,7–9]. Nevertheless, in comparison with OBE calculations, it was deemed quantitatively adequate [8,9]. It is not the point of this paper to restate this known fact. We rather wish to investigate the empirical predictions of the new formalism in the practical framework of quasi-elastic nucleon-nucleon collisions at energies around and above 1 GeV, to establish whether the new leading term approximation deviates significantly from previous works. We also plan to investigate quantitatively and systematically the effects of different layers of approximation found in several calculations. Our paper is organized as follows: in section II we introduce the general formalism, in section III we compare different approaches to the generation of soft virtual photons and discuss the differences. In section IV we explore the consequences of a better treatment of the many-body phase space. In section V, we discuss how some of the approximations seen in sections II and III can be put into perspective by an angular anisotropy analysis of the lepton spectrum. We then summarize.

II. GENERAL FORMALISM AND HADRONIC ELECTROMAGNETIC CURRENTS

Consider the reaction

$$a + b \rightarrow c + d + e^+e^- \tag{2}$$

where a, b, c, and d represent nucleons. The generic Feynman diagram for the leading-term contributions to the emission of a soft virtual photon are shown in Fig. 1. This is

the process on which we concentrate in this work. See the appendix for a mathematical description of what is a leading term and what isn't. The circle schematically represents the strong interaction. In the limit of soft photons, real or virtual, the radiation from the strong interaction blob is a sub-leading contribution. When a, b, c and d are all protons, there are eight Feynman graphs to be added coherently for the calculation of lepton pair emission. Note in passing that there have been arguments that bremsstrahlung from pn reactions should be significantly more important than that from pp. These were based on the fact that, nonrelativistically, the first non-vanishing multipole contribution for pp appears at the quadrupole level, whereas for np it is at the dipole stage. It has however been recently shown that such arguments do not hold for relativistic collisions [5]. In fact, the lepton pair yields from these two processes are comparable at 4.9 GeV [5]. There will be more on this later. Naturally, the pp bremsstrahlung contribution is crucial in the interpretation of the ratio of dileptons produced in pd and pp reactions. We will discuss pp contributions in this work, also.

We evaluate and sum the amplitudes of the relevant Feynman diagrams of the type in Fig. 1. Anticipating the soft photon limit, we assume that the hadronic part of the total matrix element is unaffected by the fact that one of its legs is slightly off-shell. We write this on-shell matrix element for elastic nucleon-nucleon scattering as $\mathcal{M}_0$. We omit the momentum labelling of the initial and final state, for simplicity. Squaring the net matrix element, $\mathcal{M}$, and summing over final state spins and averaging over initial states one obtains, under a definite set of approximations [12,13], the leading order term

$$\frac{1}{4}\sum_{s_a s_b s_c s_d s_+ s_-}|\mathcal{M}|^2 \;=\; 4\pi\alpha\overline{|\mathcal{M}_0|^2}J^\mu J^\nu L_{\mu\nu}\;. \tag{3}$$

In the above,

$$J^\mu = -Q_a\frac{(2p_a-q)^\mu}{2p_a\cdot q - M^2} - Q_b\frac{(2p_b-q)^\mu}{2p_b\cdot q - M^2} + Q_c\frac{(2p_c+q)^\mu}{2p_c\cdot q + M^2} + Q_d\frac{(2p_d+q)^\mu}{2p_d\cdot q + M^2} \tag{4}$$

is the hadron electromagnetic current, and the lepton tensor is

$$L^{\mu\nu} \;=\; \frac{8\pi\alpha}{M^4}\left(2\left(p_+{}^\mu p_-{}^\nu + p_-{}^\mu p_+{}^\nu\right) - M^2 g^{\mu\nu}\right)\;. \tag{5}$$

The Q's and p's represent charges and four-momenta for the particles, and $q^\mu = (p_+ + p_-)^\mu$. Note that $J^\mu q_\mu = 0$, as a consequence of gauge invariance. $\overline{|\mathcal{M}_0|^2}$ is the on-shell hadronic elastic scattering matrix element, squared, summed over final spins and averaged over initial spins. Again, the full details of the tedious derivation for radiating fermions is given elsewhere [12,13] and omitted here for the sake of clarity.

After performing the appropriate contractions, we may write the differential cross section for e^+e^- pair production with invariant mass M and energy q_0 as

$$E_+E_-\frac{d^6\sigma^{e^+e^-}_{ab\to cd}}{d^3p_+d^3p_-} = \frac{\alpha^2}{16\pi^5}\frac{1}{M^2}\frac{R_2(s_2,m_a^2,m_b^2)}{R_2(s,m_a^2,m_b^2)}\int[-J^2-\frac{1}{M^2}(l\cdot J)^2]\frac{d\sigma_{ab\to cd}}{dt}d\phi_c^*dt\ , \qquad (6)$$

where ϕ_c^* is the azimuthal angle of one of the outgoing hadrons in the center-of-mass frame and the four-vector $l = p_+ - p_-$ is the difference of positron and electron four-momenta and t is the four-momentum transfer. Equation (6) follows from Eq. (2.15) of [12] after specifying the nonradiative cross section as

$$d\sigma_0 = \frac{d\sigma_{ab\to cd}}{d\Omega_c}d\Omega_c = \frac{1}{2\pi}\frac{d\sigma_{ab\to cd}}{dt}d\phi_c^*dt\ , \qquad (7)$$

and including the phase-space correction introduced in [17].

In the evaluation of the original Feynman diagrams, we have neglected the four-momentum q of the virtual photon in the phase-space δ function in order to reproduce the kinematics associated with the *on-shell* elastic differential nucleon-nucleon cross section, $d\sigma/dt$ [11]. Because of this approximation, we include [17] the ratio of two-body phase space [18] $R_2(s_2,m_a^2,m_b^2)/R_2(s,m_a^2,m_b^2)$ evaluated at s_2 and s, where s is the invariant energy squared available for all the final-state particles and $s_2 = s+M^2-2q_0^*\sqrt{s}$. This approximate correction prevents the lepton pair from violating the overall energy-momentum conservation laws and thus has a significant effect on dilepton distributions. The ratio constructed from Eq. (6) with and without the correction factor correctly drops monotonically to zero in the limit of maximum invariant mass. Handling the phase-space properly is quite important. However, setting $q = 0$ in the four-dimensional delta function also forces the expression for the current to be evaluated on-shell, *i.e.* $p_c + p_d = p_a + p_b$. Clearly, this will have some

effect on the value of the current of Eq. (4). For the purpose of clarity, we will investigate separately the effects of a complete treatment of phase space in section IV.

An exercise in relativistic kinematics gets one from Eq. (6) to the Lorentz-covariant differential cross section in global dilepton variables

$$q_0 \frac{d^4\sigma^{e^+e^-}_{ab\to cd}}{dM^2 d^3q} = \frac{\alpha^2}{24\pi^4}\frac{1}{M^2}(1+\frac{2\mu^2}{M^2})\sqrt{1-\frac{4\mu^2}{M^2}}\frac{R_2(s_2,m_a^2,m_b^2)}{R_2(s,m_a^2,m_b^2)}\int(-J^2)\frac{d\sigma_{ab\to cd}}{dt}d\phi_c^* dt \qquad (8)$$

where μ is the electron mass. Our usage of Rückl's approach for dilepton production consists of neglecting the term $(p_+^\mu p_-^\nu + p_+^\nu p_-^\mu)$ of the leptonic tensor [8], Eq. (5), and analytically continuing the real photon energy to $q_0 = \sqrt{\vec{q}^2 + M^2}$. This procedure is however not Lorentz-covariant [12]. One then obtains Eq. (8) multiplied by an additional factor of 3/2 ($1+2\mu^2/M^2)^{-1}$. From here on, we shall discuss electron-positron pair production exclusively and we systematically will use $\mu = 0$.

To complete our analysis of previous efforts we now turn our attention to the electromagnetic current. For emission of real photons in reaction (2), the current is

$$J^\mu = -Q_a\frac{p_a^\mu}{p_a\cdot q} - Q_b\frac{p_b^\mu}{p_b\cdot q} + Q_c\frac{p_c^\mu}{p_c\cdot q} + Q_d\frac{p_d^\mu}{p_d\cdot q}. \qquad (9)$$

This approximation was also used by several authors, in the case of soft *virtual* photons [16,3,19,4,5]. It is worth mentioning here that for the case of virtual photons, the "soft" limit is not unambiguously defined: for virtual photons, what is meant by a "soft photon limit"? Here, we use this term in connection with the condition $M \to 0$. However, bear in mind that the lepton pair energy and lepton pair three-momentum can individually still be quite large. Thus $M \to 0$ is in fact not a sufficient condition to neglect both q_0 and $\vec{q}$ in the delta functions, even if this omission can *partially* be corrected (*e.g.* Eq. (6)). The opposite limit where M is large implies that the lepton pair energy is large and most certainly can't be ignored in the phase space delta function. By the same token, off-shell effects on the strong interaction amplitude can be small in the $M \to 0$ limit, but won't be, in the large M region. In this work we do not include a discussion of off-shell effects. We should however keep this point in mind when discussing the regions of validity of our calculations.

There are thus several possible ingredients that can affect the results of lepton pair emission calculations of the "soft photon type". One resides in the use of the Rückl formula, a widely-used expression which nevertheless is not Lorentz-covariant. This first point is easily settled: our interpretation of Rückl's formula for electron-positron pair production instead of Eq. (8) simply introduces an overall factor of 3/2. Another possible source of disagreement between calculations has to do with the use of the current of Eq. (9) as the electromagnetic current for hadrons when *massive* lepton pairs are emitted. For lepton pairs with very small invariant masses the current represented by Eq. (4) of course reduces to that of Eq. (9). Also, the exact treatment of dynamics will play a role. For the time being, we set $q = 0$ in the four-dimensional Dirac delta function and simply use the phase space correction factor associated with Eq. (6). In the next section, we investigate the effects of using different hadronic electromagnetic currents.

III. COMPARING CURRENTS

Squaring the current (4), as is required by Eq. (8), we obtain an expression that depends on the spatial orientation of the virtual photon. Taking an angular average, and for an equal-mass reaction of the type specified in Eq. (2) with $m_a = m_b = m_c = m_d = m$, we arrive at

$$\begin{aligned}
-J^2 = \frac{1}{q_0^2}\Bigg\{ & -[\lambda_1^2(Q_a^2+Q_b^2)\frac{4m^2-M^2}{s(1-\beta_a'^2)} + \lambda_2^2(Q_c^2+Q_d^2)\frac{4m^2-M^2}{s(1-\beta_c'^2)}] \\
& -2\lambda_1^2 Q_a Q_b(2-\frac{M^2}{s}-\frac{4m^2}{s})F(\vec{\beta}_a',\vec{\beta}_b') \\
& -2\lambda_2^2 Q_c Q_d(2-\frac{M^2}{s}-\frac{4m^2}{s})F(\vec{\beta}_c',\vec{\beta}_d') \\
& +2\lambda_1\lambda_2(Q_aQ_c+Q_bQ_d)\frac{4m^2+M^2-2t}{s}F(\vec{\beta}_a',\vec{\beta}_c') \\
& +2\lambda_1\lambda_2(Q_aQ_d+Q_bQ_c)\frac{2s+M^2-4m^2+2t}{s}F(\vec{\beta}_a',\vec{\beta}_d')\Bigg\},
\end{aligned} \tag{10}$$

where the function

$$F(\vec{x},\vec{y}) = \frac{1}{2\sqrt{R}}\ln\left|\frac{[\vec{x}\cdot\vec{y}-x^2-\sqrt{R}][\vec{x}\cdot\vec{y}-y^2-\sqrt{R}]}{[\vec{x}\cdot\vec{y}-x^2+\sqrt{R}][\vec{x}\cdot\vec{y}-y^2+\sqrt{R}]}\right|, \tag{11}$$

and where the radicand is

$$R = (1 - \vec{x} \cdot \vec{y})^2 - (1 - x^2)(1 - y^2). \tag{12}$$

To make the formula more compact, we have introduced the variables

$$\lambda_1 = \frac{1}{1 - M^2/\sqrt{s}q_0}, \quad \lambda_2 = \frac{1}{1 + M^2/\sqrt{s}q_0}, \quad \gamma = 1 - \frac{M^2}{q_0^2}. \tag{13}$$

The velocities β are related to the above definitions and to invariants through

$$\begin{aligned}
&\beta_a'^2 = \beta_b'^2 = \lambda_1^2\gamma(1 - \frac{4m^2}{s}), \quad \beta_c'^2 = \beta_d'^2 = \lambda_2^2\gamma(1 - \frac{4m^2}{s}), \\
&\vec{\beta}_a' \cdot \vec{\beta}_b' = -\lambda_1^2(1 - \frac{4m^2}{s}), \quad \vec{\beta}_c' \cdot \vec{\beta}_d' = -\lambda_2^2(1 - \frac{4m^2}{s}), \\
&\vec{\beta}_a' \cdot \vec{\beta}_c' = -\vec{\beta}_a' \cdot \vec{\beta}_d' = \lambda_1\lambda_2\gamma(1 - \frac{4m^2}{s} + \frac{2t}{s}).
\end{aligned} \tag{14}$$

Notice that terms directly proportional to $1/q_0$ have exactly cancelled and disappeared upon squaring the current. If we set $M = 0$ in Eq. (10), we recover Eq.(3.6) of Ref. [20].

We have calculated the ratio $R_0 = -J^2_{\text{virtual}} / -J^2_{\text{real}}$ with the angular-averaged currents of Eq. (4) and Eq. (9). This ratio depends on the invariant energy s, the four-momentum transfer t, and the dilepton invariant mass and energy: M and q_0. For the purpose of comparison, we arbitrarily input some reasonable values and plot R_0 against the virtual photon three-momentum in Fig. 2. We find sizeable deviations from 1 in this quantity. The ratio for pn processes is sensitive to the value of $\theta_{\text{c.m.}}$, the scattering angle in the nucleon-nucleon centre of mass, whereas it is quite insensitive for the pp case. Interference effects evidently play a role here. To better understand the effect of the "complete" current (also labelled "virtual", above) on the differential cross section for dilepton production, we integrate over t and plot $R_1 = (\frac{d\sigma}{dM^2d^3q})_{\text{virtual}}/(\frac{d\sigma}{dM^2d^3q})_{\text{real}}$ as a function of the c.m. virtual photon momentum $|\vec{q}|$ in Fig. 3, for different dilepton invariant masses. We are now essentially comparing the effect of using Eq. (4) over Eq. (9) in a dilepton production calculation. Also, to actually compare two sets of calculations that have been done previously, the numerator is derived from Eq. (8), while the denominator is derived from Rückl's approach.

Before discussing the results in Fig. 3, let us restate that the net lepton pair spectrum will depend on the details of the differential nucleon-nucleon elastic cross-section, $d\sigma/dt$. This is evident from Eq. (6) and Eq. (8). It thus follows that the present analysis will have to be redone for different systems at different energies, with possibly different conclusions. For example, quark-quark and pion-pion virtual bremsstrahlung calculations have attracted some recent attention in connection with ultrarelativistic heavy-ion collisions [20,21]. The consequences of the present formalism on such studies is presently being analyzed [22]. It is thus imperative to have an accurate parametrization for the elastic nucleon-nucleon differential cross section $d\sigma/dt$ over the relevant range in t. For pn elastic collisions, $d\sigma/dt$ is nearly symmetric for kinetic energy less than 1 GeV. But at higher energies, the observed distributions are not symmetric about $\theta_{c.m.} = 90°$ but rather develop a stronger forward peak. This asymmetry increases with the scattering energy and can suppress the pn bremsstrahlung contribution to dilepton production by a factor of 4 at 4.9 GeV [10,5]. A fairly detailed parametrization at 4.9 GeV kinetic energy was used in Ref. [5] to calculate the absolute sizes of the pn and pp bremsstrahlung contributions. For practical reasons, we instead adopt the parametrizations of Refs. [10] and [23] for the pn and pp elastic differential cross sections. These two functional forms can fit the experimental data for energies up to 6 GeV with the necessary accuracy.

Analyzing Fig. 3, the ratio R_1 remains 2/3 for small invariant mass $M \leq 10$ MeV. For higher invariant masses, R_1 is greater than 2/3 for almost all values of the virtual photon momentum, in the case of pn scattering. Increasing M in the pp case, R_1 remains still considerably smaller than 2/3 at low momenta and drastically increases as the three-momentum grows. The low-momentum value of R_1 is thus quite different in the two reactions at hand. It is not simple to draw clear physical conclusions for these behaviours, but the main point is that these features suggest that using the "complete" current for virtual photons changes the distribution of the dielectrons in phase space, especially in the pp case.

Upon integration, we arrive at differential cross sections in terms of lepton pair invariant mass. In Fig. 4, we show two curves: the dashed curve corresponds to using the Rückl

formula with the real photon current, Eq. (9). The solid curve corresponds to using Eq. (8) with the current of Eq. (4). In each panel three kinetic energies are shown: 1.0, 3.0 and 4.9 GeV. We are thus in effect evaluating the difference between two approaches to calculating the dielectron production in nucleon-nucleon collisions: the one based on Rückl's equation and the real photon current (we remind the reader that this combination has become well known and widely used), and the one based on the more recent Lorentz-covariant formalism with a more general electromagnetic current for hadrons. At these energies (which correspond to DLS measurements) one realizes that the Lorentz-covariant and gauge-invariant formulæ that we adopted in this work (solid curves) reduce the dilepton production cross section only slightly for $M < 0.5$ GeV in both *pn* and *pp* processes compared with previous results. For $M > 0.5$ GeV, the situation is a little more complicated as a slight decrease or a slight increase is observed, depending on the beam energy. We have verified that the ratio $(\frac{d\sigma}{dM^2})_{\rm virtual}/(\frac{d\sigma}{dM^2})_{\rm real}$ is equal to 2/3 in the small M region for both *pn* and *pp* cases, and found it to increases monotonically with M for *pn* process, but decreases monotonically for *pp* as one goes toward the kinematical limit. Recall that other physical processes dominate the dielectron yield for $M > 0.5$ GeV at large enough beam energy [5]. In the large invariant mass region, Fig. 4 suggests that the previous bremsstrahlung calculations underestimate the dilepton yields at most by a factor of 2 even at the kinetic energy 4.9 GeV, even though our formalism is not strictly applicable there. For *pp* scattering, it is worthwhile to point out that the radiation intensity is strongly depleted due to interference effects near the maximum M.

Thus our findings at this point are essentially these: the "improved" formalism does not affect very much the soft lepton yields previously calculated. We do not address in detail the issue of hard leptons ($M \geq 0.5$ GeV) because there, the present formalism is inadequate. In the small invariant mass region $M < 0.5$ GeV, we find that this new formalism only amounts to the numerical difference of 2/3.

We have made above a formal comparison of two approaches. However, we did discover that the two formalisms would produce different phase space distributions of lepton pairs:

see Fig. 3. Let us now consider the specific case of DLS measurements. It is a known fact that any theoretical calculation attempting to reproduce the DLS data should first be filtered by the DLS experimental acceptance. It is then conceivable that the predictions of the two approaches could be affected quite differently by the experimental filter. We have run our two sets of calculations through the DLS experimental filter [24]. In Fig. 5 we show the invariant mass dependence of the absolute differential cross sections, at kinetic energies 1.0, 3.0 and 4.9 GeV. This figure now suggests that the previous calculations overestimated the low-mass dielectron yields by a factor of 2-3 for np and a factor of 2-5 for pp bremsstrahlung in collisions at 4.9 GeV. Thus the effect of the DLS acceptance is to make the differences between the two approaches more pronounced. The effect is smaller for lower kinetic energies. We refrain here from making specific data comparisons. For these, important sources such as π-π annihilation, η Dalitz decay and Δ radiative decay have to be included. The latter two can be incorporated incoherently in our approach, keeping in mind that interference effects might be important [25]. Also, many-body bremsstrahlung has been shown to be quantitatively important at 4.9 GeV [5].

Another useful comparison is the relative radiative intensities of pp and np scattering. As mentioned above, pp bremsstrahlung has often been neglected because of a classical multipole argument. We calculate the ratio here, with the formalism based on the leading-term approximation, *i.e.* with Eq. (8) and Eq. (4). The relative intensities depend on kinetic energy as shown in Fig. 6 which presents the ratio $R = (\frac{d\sigma}{dM^2})_{\rm pp}/(\frac{d\sigma}{dM^2})_{\rm pn}$ as a function of invariant mass at different kinetic energies. Proton-proton bremsstrahlung becomes more and more important as the kinetic energy increases. At 2 GeV, for instance, R is nearly 0.5 for small masses whereas at 4.9 GeV it becomes larger than 1. We shall return to this ratio in the next section.

IV. ONE STEP FURTHER: THE EXACT TREATMENT OF PHASE SPACE

In all of the above comparisons, we have consistently set $q = 0$ in the 4-dimensional phase space delta function. We now avoid making this approximation and investigate the consequences. The many-body Lorentz-invariant phase space can be expressed in terms of Mandelstam-type invariants [18], or in this case one can perform the integrals directly [26]. Going back one step, let's write the general equation that leads to Eq. (6), without its phase space correction. In the process $a+b \to c+d+e^+e^-$, the differential cross section for lepton pair production with invariant mass M and energy q_0 is

$$E_+E_-\frac{d^6\sigma^{e^+e^-}_{ab\to cd}}{d^3p_+d^3p_-} = \frac{1}{4E_aE_b|\mathbf{v}_a-\mathbf{v}_b|}\frac{\alpha^2}{8\pi^4}\frac{1}{M^2}\int[-J^2-\frac{1}{M^2}(l\cdot J)^2] \times \overline{|\mathcal{M}_0|^2}(2\pi)^4\delta^4\left(p_a+p_b-p_c-p_d-q\right)\frac{d^3p_c}{(2\pi)^32E_c}\frac{d^3p_d}{(2\pi)^32E_d}\,, \tag{15}$$

where $\overline{|\mathcal{M}_0|^2}$ is the on-shell matrix element for the scattering $a+b \to c+d$, squared, summed over final spins and averaged over initial spins. The differential cross section can be rewritten as

$$q_0\frac{d^4\sigma^{e^+e^-}_{ab\to cd}}{dM^2d^3q} = \frac{1}{4E_aE_b|\mathbf{v}_a-\mathbf{v}_b|}\frac{\alpha^2}{48\pi^5}\frac{1}{M^2}(1+\frac{2\mu^2}{M^2})\sqrt{1-\frac{4\mu^2}{M^2}} \times \int(-J^2)\overline{|\mathcal{M}_0|^2}\delta^4\left(p_a+p_b-p_c-p_d-q\right)\frac{d^3p_c}{2E_c}\frac{d^3p_d}{2E_d}\,, \tag{16}$$

where μ is the rest mass of an individual lepton. In the $a+b$ centre of mass frame, one may perform some of the integrals and get

$$\int\delta^4\left(p_a+p_b-p_c-p_d-q\right)\frac{d^3p_c}{2E_c}\frac{d^3p_d}{2E_d} = \frac{1}{4}\int\delta\left(\cos\theta_{p_dq}-\frac{s+M^2+2E_dq_0-2\sqrt{s}(E_d+q_0)}{2|\vec{p}_d||\vec{q}|}\right) \times \frac{1}{|\vec{q}|}dE_d d\cos\theta_{p_dq}d\phi_{p_d}\,. \tag{17}$$

Furthermore, in the on-shell limit, the squared matrix element summed over final spins and averaged over initial spins can be related to the on-shell differential elastic cross section by

$$\overline{|\mathcal{M}_0|^2} = 16\pi s(s-4m^2)\frac{d\sigma}{dt}\,. \tag{18}$$

Integrating further, one obtains

$$\frac{d\sigma^{e^+e^-}}{dM^2} = \frac{\alpha^2}{24\pi^4}\frac{1}{M^2}(1+\frac{2\mu^2}{M^2})\sqrt{1-\frac{4\mu^2}{M^2}}\sqrt{s(s-4m^2)}\int(-J^2)\frac{d\sigma_{ab\to cd}}{dt}$$
$$\times\,\delta\left(\cos\theta_{p_dq}-\frac{s+M^2+2E_dq_0-2\sqrt{s}(E_d+q_0)}{2|\vec{p_d}||\vec{q}|}\right)$$
$$dq_0dE_d d\Omega_q d\cos\theta_{p_dq}d\phi_{p_d}\ . \tag{19}$$

The range of the integration variables is such that the condition

$$|\cos\theta_{p_dq}| = \left|\frac{s+M^2+2E_dq_0-2\sqrt{s}(E_d+q_0)}{2|\vec{p_d}||\vec{q}|}\right| \leq 1 \tag{20}$$

has to be satisfied.

With the help of gauge invariance, it is not very difficult to write the 4-current squared in terms of ten scalar products $p_i \cdot p_j$. Setting $m_a = m_b = m_c = m_d = m$, we obtain

$$-J^2 = -\frac{Q_a^2(4m^2-M^2)}{(2p_a\cdot q-M^2)^2} - \frac{Q_b^2(4m^2-M^2)}{(2p_b\cdot q-M^2)^2} - \frac{Q_c^2(4m^2-M^2)}{(2p_c\cdot q+M^2)^2} - \frac{Q_d^2(4m^2-M^2)}{(2p_d\cdot q+M^2)^2}$$
$$-\frac{2Q_aQ_b(4p_a\cdot p_b-M^2)}{(2p_a\cdot q-M^2)(2p_b\cdot q-M^2)} + \frac{2Q_aQ_c(4p_a\cdot p_c+M^2)}{(2p_a\cdot q-M^2)(2p_c\cdot q+M^2)}$$
$$+\frac{2Q_aQ_d(4p_a\cdot p_d+M^2)}{(2p_a\cdot q-M^2)(2p_d\cdot q+M^2)} + \frac{2Q_bQ_c(4p_b\cdot p_c+M^2)}{(2p_b\cdot q-M^2)(2p_c\cdot q+M^2)}$$
$$+\frac{2Q_bQ_d(4p_b\cdot p_d+M^2)}{(2p_b\cdot q-M^2)(2p_d\cdot q+M^2)} - \frac{2Q_cQ_d(4p_c\cdot p_d-M^2)}{(2p_c\cdot q+M^2)(2p_d\cdot q+M^2)}\ . \tag{21}$$

In the $a+b$ centre of mass, the scalar products can be written in terms of the integration variables of Eq. (19). For instance, writing $|\vec{p_a}| = |\vec{p_b}| = |\vec{p}| = \sqrt{s/4-m^2}$ and the energy $E_a = E_b = E = \sqrt{s}/2$, then $p_a\cdot p_b = E^2+|\vec{p}|^2$; $p_a\cdot q = Eq_0 - |\vec{p}||\vec{q}|\cos\theta_{p_aq}$; $p_d\cdot q = E_dq_0 - |\vec{p_d}|\vec{q}|\cos\theta_{p_dq}$; and $p_a\cdot p_d = EE_d - |\vec{p}||\vec{p_d}|(\cos\theta_{p_aq}\cos\theta_{p_dq}+\sin\theta_{p_aq}\sin\theta_{p_dq}\sin\phi_{p_d})$. All other scalar products involve the above four.

On Fig. 7 we display three different curves for the cases of pn and pp scattering, at energies of 1.0, 3.0 and 4.9 GeV. We compare calculations done with Eq. (19), calculations done using Rückl's formula with the current of Eq. (9), and calculations done using Eq. (8) together with the current of Eq. (4). The three approaches display behaviors that are quite similar and are not really remarkably different. The largest deviations occur at the lowest bombarding energies at low M. Recall that the "soft photon limit" is not really properly defined by $M \to 0$. Running our results through the DLS acceptance filter, in Fig. 8, one

realizes that the results obtained with Eq. (19), and those obtained with Eq. (8) together with the current of Eq. (4) are very similar for the pn reactions. The only exception there is the low energy pn spectrum at low invariant masses. In the case of pp, the filter effects are such that the results with the complete phase space are lower than the previous ones at high invariant masses. The effect of the DLS acceptance brings us to the conclusion that the position of the lepton pairs in phase space is mostly determined by the nature of the electromagnetic current, once the on-shell nucleon-nucleon cross section is fixed. The pp/np ratio does however show some sensitivity to the treatment of phase space, as displayed in Fig. 9.

There is no question that the current of Eq. (4) is more general and appropriate for leptons than that of Eq. (9). In a given reaction the differences in dilepton invariant cross sections, before filtering, that follow the use of those two currents are not minuscule but can not be called spectacular. There is an observable that has a remarkably different behavior, whether or not the current (4) is used in calculations. We elaborate more on this in the following section.

V. THE ANGULAR DISTRIBUTION OF BREMSSTRAHLUNG DILEPTONS

We have already mentioned that the nature of the electromagnetic current for the bremsstrahlung producing hadrons will greatly affect the position of the leptons in phase space. This already became clear in our analysis of Fig. 3. Thus, it is very reasonable that the differences in currents could be highlighted in a treatment focusing on the fine points of angular distributions, for example. Angular anisotropies have recently been put forward as a means of distinguishing between competing lepton pair production sources [27]. This argument has power only if the angular distributions of those sources can reliably be calculated. Let's elaborate on this below.

Owing to collision dynamics, the polarization of the virtual photon eventually converting into a lepton pair may be such that, in the rest frame of the dilepton, the single lepton

distribution may not be isotropic. This is the essence of the idea. Following [27], we write the differential cross section for emission of a lepton pair of invariant mass M, with a lepton coming out at a polar angle θ in the rest frame of the lepton pair as

$$S(M,\theta) = \frac{d\sigma}{dM^2 d\cos\theta} = A(1 + B\cos^2\theta) \ . \tag{22}$$

This enables us to write the polar anisotropy coefficient, B, as

$$B = \frac{S(M,\theta = 0^\circ)}{S(M,\theta = 90^\circ)} - 1 \ . \tag{23}$$

Since the full phase is obviously crucial to the proper kinematics, we use the methods of the previous section. The cross section to be used in the definition of S, above, is obtained by noting that for electron-positron pair production [12],

$$q_0 \frac{d^6\sigma^{e^+e^-}}{dM^2 d^3q d\tilde{\Omega}_+} = \frac{1}{4} E_+ E_- \frac{d^6\sigma^{e^+e^-}}{d^3p_+ d^3p_-} \ , \tag{24}$$

where q_0 is the lepton pair energy and $\tilde{\Omega}_+$ is the solid angle element for positron emission in the rest frame of the lepton pair. With the help of the above equation, one can numerically integrate Eq. (15) into the required format. In the on-shell approximation we are using for the strong matrix element, where $\mathcal{M}_0$ has no dependence on q, the anisotropy coefficient B only depends on kinematics and on the electromagnetic current. Details of the strong interaction do not influence it. We have numerically confirmed this by varying the strong interaction differential cross section and observing the constancy of B.

We first investigate the polar anisotropy of the lepton distribution using the current associated with Eq. (9). The results are shown in Fig. 10. We plot the coefficient B as a function of invariant mass, for different incident kinetic energies. Those energies are 1, 2, 3, and 5 GeV. They can be readily identified in the figure by their kinematical limit moving to higher invariant mass as the beam energy grows. The calculations are for bremsstrahlung in pn collisions. Our results at 1 and 2 GeV reproduce those of Ref. [27]. Repeating the calculation with the full current of Eq. (4), we see our results change drastically, both qualitatively and quantitatively. This is now plotted in Fig. 11. The anisotropy coefficients

no longer cross zero roughly together at about $M = 0.25$ GeV. The crossing points have spread out, and an important feature is that the curves have all been shifted upwards. The anisotropy coefficients are now mostly positive, except in the high invariant mass region of the last two incident kinetic energies. Also, the minima have been shifted to higher invariant masses. Thus, it is clear that any physical interpretation relying on the angular anisotropy of the lepton spectrum will thus depend on the details of the calculation. In this observable, the differences in electromagnetic currents clearly stand out.

For the case of pp bremsstrahlung, the use of the complete current is absolutely crucial. The current of Eq. (9) is used to compute the polar anisotropy coefficient plotted in Fig. 12. The current of Eq. (4) is used to compute the curves appearing in Fig. 13. The difference is striking. With the complete current, the pp signal bears some resemblance to its pn counterpart, whereas the current associated with real photons yields a complete different picture, both qualitatively and quantitatively.

VI. SUMMARY

In summary, we have used a Lorentz-covariant and gauge-invariant formalism to calculate lepton pair production cross sections via pn and pp bremsstrahlung, in the leading term approximation. The exact squared current derived for virtual photons is suitable for any energy and for any two-body equal-mass system. With the appropriate generalizations one could apply it to an unequal mass system and to reactions involving many-body final states. This is important and should be done. We find that using the complete current for virtual photons will produce differential dilepton cross sections that are not very different from those obtained using the real photon current. Since the exact virtual photon current changes the momentum distributions of the dileptons, the differences are somewhat accentuated by running the calculations through the DLS acceptance filter. However, the different phase space population associated with the different currents emerge in a much more striking fashion when plotting the polar anisotropy coefficient for leptons in the lepton pair rest

frame. We feel that the lepton angular anisotropy might in fact be useful in the identification of different sources, but only once the calculations are deemed to possess the required level of reliability and precision.

We do not suggest that the DLS bremsstrahlung analyses have to be completely redone. However, larger differences in the approaches (the one based on Rückl's formula and the Lorentz-covariant one) do show up in the pp channel, comparing with the pn channel. Thus to pin down the various mechanisms for dilepton production more precisely and to compare quantitatively to data, it does seem necessary to scrutinize some of the previous bremsstrahlung estimates, as our results suggest that some of them might have somewhat overestimated the low-mass yields.

The relative bremsstrahlung intensities from pp and pn scattering have been an actively debated issue for some time. We provided a practical and quantitative way to illustrate this, for kinetic energies up to 6 GeV. Our results suggest that pp bremsstrahlung is quite important when the kinetic energy is higher than roughly 2 GeV.

Acknowledgments

We are happy to acknowledge discussions and a useful correspondence with P. Lichard. We thank him for suggesting changes in the first version of this paper. We also acknowledge useful discussions with H. Eggers and O. V. Teryaev. This work has been supported in part by the Natural Sciences and Engineering Research Council of Canada, by the FCAR fund of the Québec Government, by a NATO Collaborative Research Grant, and by the National Science Foundation under grant number 94-03666.

REFERENCES

[1] See, for example, Proceedings of the Workshop on Dilepton Production in Relativistic Heavy Ion Collisions, March 2-4, 1994, GSI, Darmstadt, Germany; edited by H. Bokemeyer.

[2] G. Roche *et al.*, Phys.Rev.Lett. **61**, 1069 (1988);G. Roche *et al.*, Phys. Lett. **B 226**, 228 (1989);C. Naudet et al., Phys. Rev. Lett. **62**, 2652 (1989).

[3] L. Xiong, Z.G. Wu, C.M. Ko and J.Q. Wu, Nucl. Phys. **A 512**, 772 (1990).

[4] Gy. Wolf, G. Batko, W. Cassing, U. Mosel, K. Niita and M. Schäfer, Nucl. Phys. **A 517**, 615 (1990) .

[5] Kevin Haglin and Charles Gale, Phys. Rev. **C 49**, 401 (1994).

[6] W.K. Wilson et al., Phys. Lett. **B 316**, 245 (1993).

[7] Kevin Haglin, Joseph Kapusta, and Charles Gale, Phys Lett. **B 224**, 433 (1989).

[8] M. Schäfer, T. S. Biro, W. Cassing, and U. Mosel, Phys. Lett. **B 221**, 1 (1989).

[9] Kevin L. Haglin, Ann. Phys. (N. Y.) **212**, 84 (1991).

[10] L.A. Winckelmann, H. Stöcker and W. Greiner, Phys. Lett. **B 298**, 22 (1993).

[11] See, for example, J. D. Bjorken and S. D. Drell, *Relativistic Quantum Mechanics* (McGraw-Hill, New York, 1964).

[12] P. Lichard, Phys. Rev. **D 51**, 6017 (1995).

[13] The two-fermion case of Ref. [12] is generalized to four fermions in R. Tabti, MSc thesis (unpublished), McGill University 1995.

[14] R. Rückl, Phys. Lett. **B 64**, 39 (1976).

[15] V. Balek, N. Pišúova and J. Pišút, Acta Phys. Slovaca **41**, 224 (1991).

[16] C. Gale and J. Kapusta, Phys. Rev. **C 35**;2107 (1987).

[17] C. Gale and J. Kapusta, Phys Rev. **C 40**, 2397 (1989) .

[18] E. Byckling and K. Kajantie, *Particle Kinematics* (Wiley, New York, 1973).

[19] L. Xiong, J. Q. Wu, Z. G. Wu, C. M. Ko, and J. H. Shi, Phys. Rev. **C 41**, R1355 (1990).

[20] K. Haglin, C. Gale, and V. Emel'yanov, Phys. Rev. **D 47**, 973 (1993).

[21] J. Cleymans, V. V. Goloviznin, and K. Redlich, Phys. Rev. **D 47**, 989 (1993).

[22] H. C. Eggers, R. Tabti, C. Gale, and K. Haglin, report McGill/95-14, HEPHY-PUB 620/95, MSUCL-974.

[23] R.L. Hatch, Ph.D Thesis, California Institute of Technology, 1980, (unpublished).

[24] We have used DLS filter version 2.0, provided by the experimental collaboration.

[25] M. Schäfer, H. C. Dönges, A. Engel, and U. Mosel, Nucl. Phys. **A 575**, 429 (1994).

[26] A. I. Titov, B. Kämpfer, and E. L. Bratkovskaya, Phys. Rev. **C 51**, 227 (1995).

[27] E. L. Bratkovskaya, O. V. Teryaev, and V. D. Toneev, Phys. Lett. **B 348**, 283 (1995).

FIGURES

FIG. 1. The leading contributions for dilepton radiation in the reaction $a + b \rightarrow c + d + e^+e^-$.

FIG. 2. The ratio $R \equiv -J^2_{\rm virtual} / -J^2_{\rm real}$ and its dependence on the center-of-mass dilepton momentum $q = |\vec{q}|$ and hadron scattering angle θ for (a) pn, and (b) pp processes at kinetic energy 4.9 GeV and invariant mass $M = 0.2$ GeV.

FIG. 3. The ratio of the differential cross section $R_1 \equiv (\frac{d\sigma}{dM^2 d^3q})_{\rm virtual} / (\frac{d\sigma}{dM^2 d^3q})_{\rm real}$ as a function of the center-of-mass dilepton momentum q for (a) np, and (b) pp processes, at kinetic energy 4.9 GeV and for dilepton invariant masses M= 0.01, 0.2, 0.6 and 0.8 GeV, respectively.

FIG. 4. The differential cross section for dilepton production from (a) pn and (b) pp collisions versus the dilepton invariant mass M. The solid lines are results using the virtual photon formalism described in the text, the dotted lines are the results obtained using Rückl's formula together with the current for real photons. Results for kinetic energies $E_{\rm kin}$= 1.0, 3.0, and 4.9 GeV are shown. For clarity of presentation, the results have been multiplied by a scaling factor. The scaling factor is 1 at 1 GeV, 10 at 3.0 GeV and 100 at 4.9 GeV.

FIG. 5. The same as in Fig. 4, but with the correction of the acceptance filter. The solid symbols are with the formalism of Eq. (8) together with the current of Eq. (4), while the open symbols are the results of using Rückl's formula together with the current for real photons.

FIG. 6. The ratio of dilepton production cross sections in pp and np reactions, $R = (\frac{d\sigma}{dM})_{\rm pp} / (\frac{d\sigma}{dM})_{\rm pn}$, as a function of invariant mass M at kinetic energies 1.0, 2.0, 3.0 and 4.9 GeV, from bottom to top.

FIG. 7. We plot the differential cross section for production of lepton pairs of invariant M in the cases of pn (left panel) and pp collisions (right panel) at incident kinetic energies of 1, 3, and 4.9 GeV (bottom to top curves, respectively). The full curves represent calculations done with Eq. (19), the short-dashed curves are generated with the formula of Rückl, together with the current for real photons, and the long-dashed curves are done using Eq. (8) together with the current of Eq. (4). The scaling factors are as in Fig. 4.

FIG. 8. The same as Fig. 7, but with the DLS acceptance corrections. The open triangles are the results of using Rückl's formula together with the current for real photons. The open circles are associated with Eq. (8) together with the current of Eq. (4). The solid triangles are generated with Eq. (19).

FIG. 9. Same caption as Fig. 6, only this time the complete phase space approach of section IV is used.

FIG. 10. We plot the polar anisotropy coefficient, as defined in the text, against lepton pair invariant mass for incident kinetic energies of 1, 2, 3, and 5 GeV in pn collisions. We use the current of Eq. (9).

FIG. 11. Same caption as Fig. 10. We use here the current of Eq. (4).

FIG. 12. Same caption as Fig. 10, but for pp collisions.

FIG. 13. Same caption as Fig. 11, but for pp collisions.

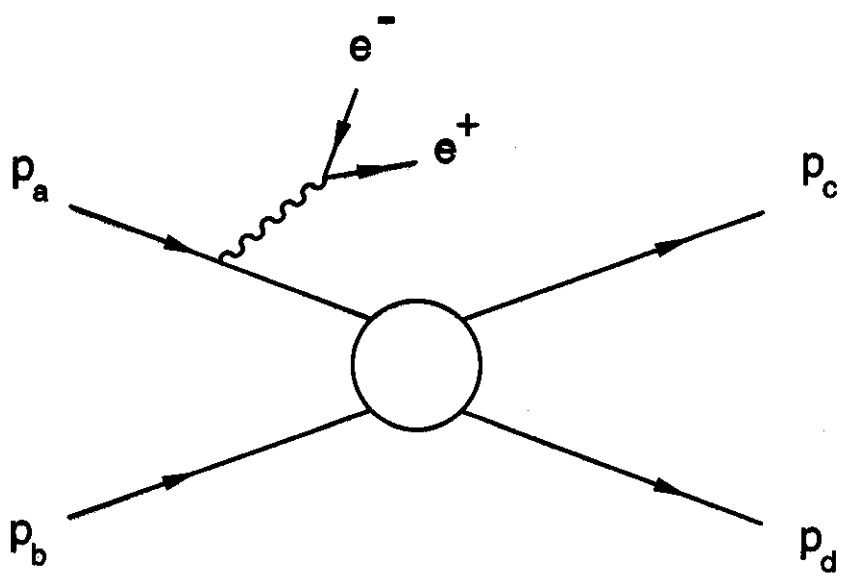

+ contributions from
other charged lines

Figure 1

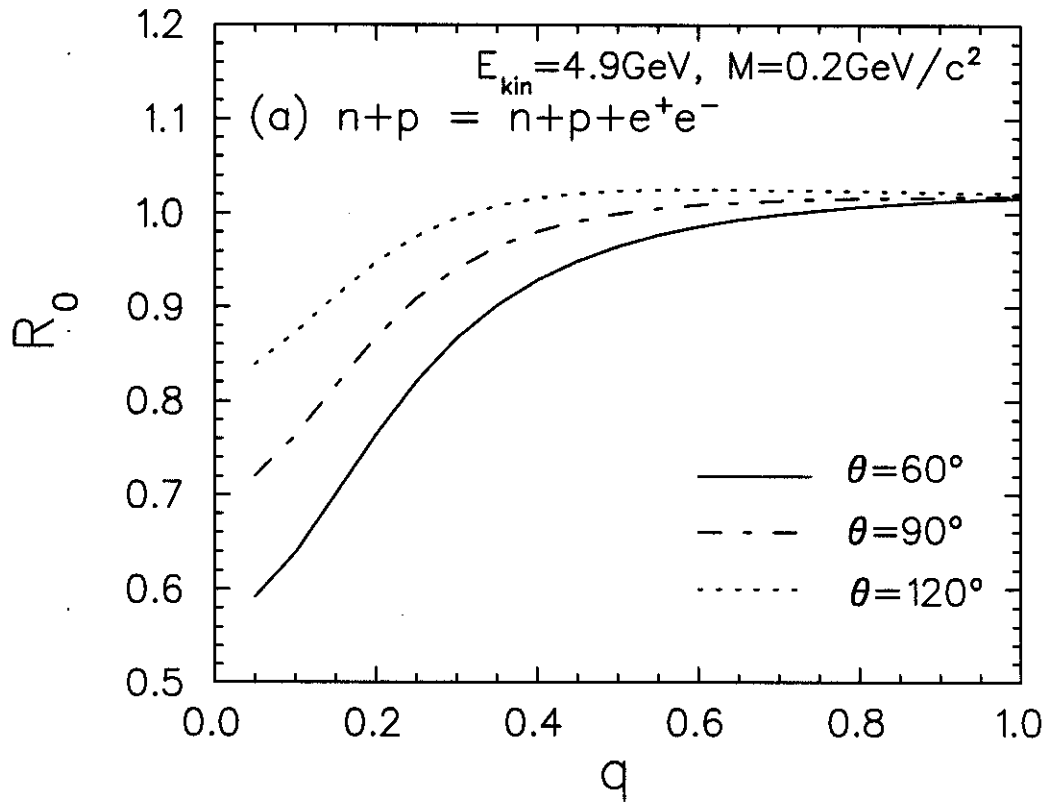
E_{kin}=4.9GeV, M=0.2GeV/c^2
(a) n+p = n+p+e^+e^-
R_0
q
θ=60°
θ=90°
θ=120°

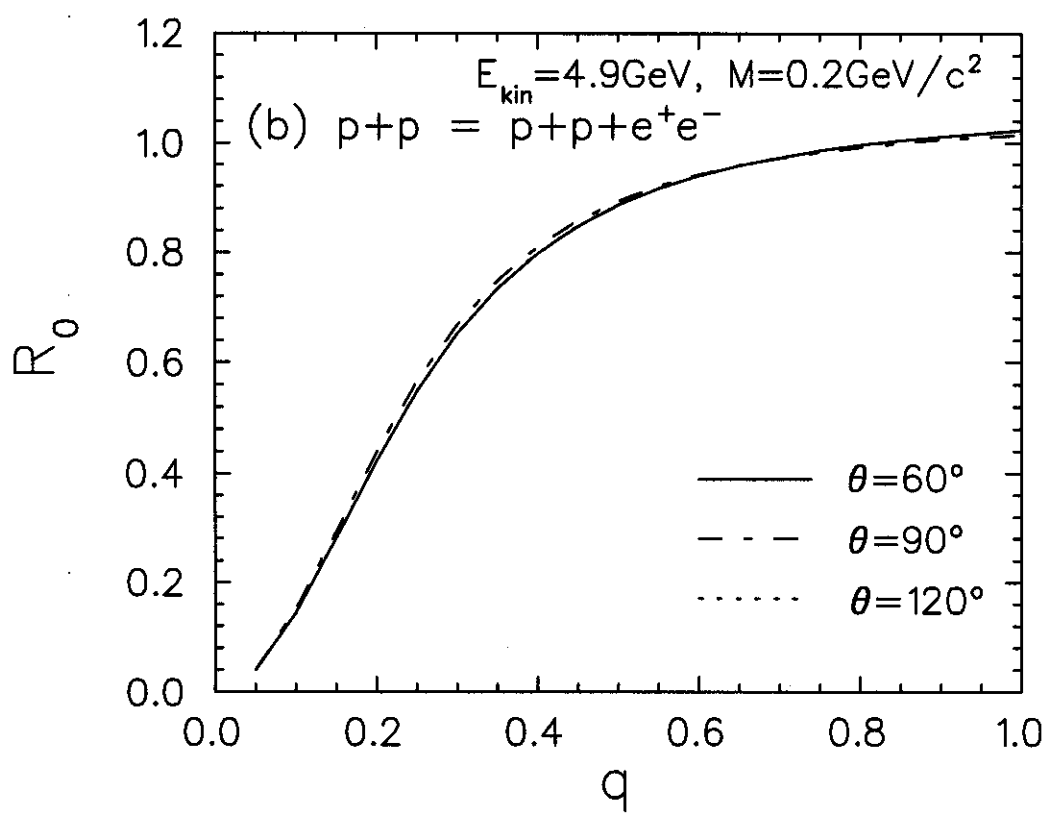
E_{kin}=4.9GeV, M=0.2GeV/c^2
(b) p+p = p+p+e^+e^-
R_0
q
θ=60°
θ=90°
θ=120°

Fig. 2

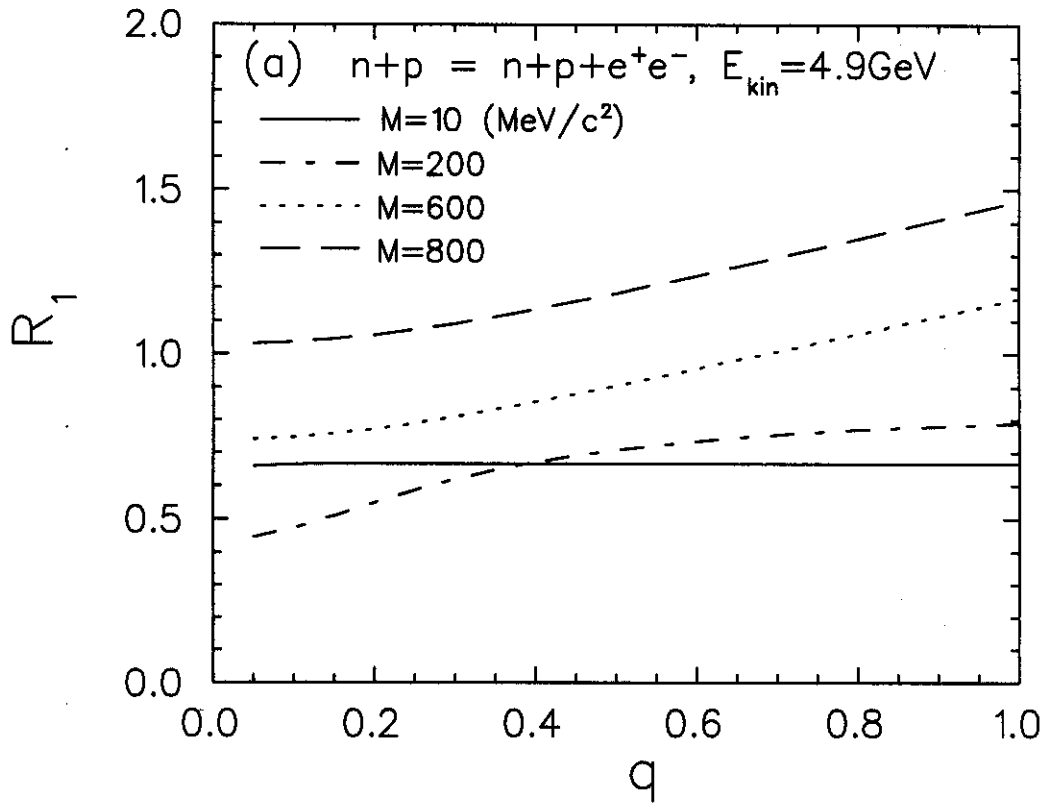
(a) n+p = n+p+e+e−, Ekin=4.9GeV
M=10 (MeV/c²)
M=200
M=600
M=800
R1
q
0.0
0.5
1.0
1.5
2.0
0.2
0.4
0.6
0.8

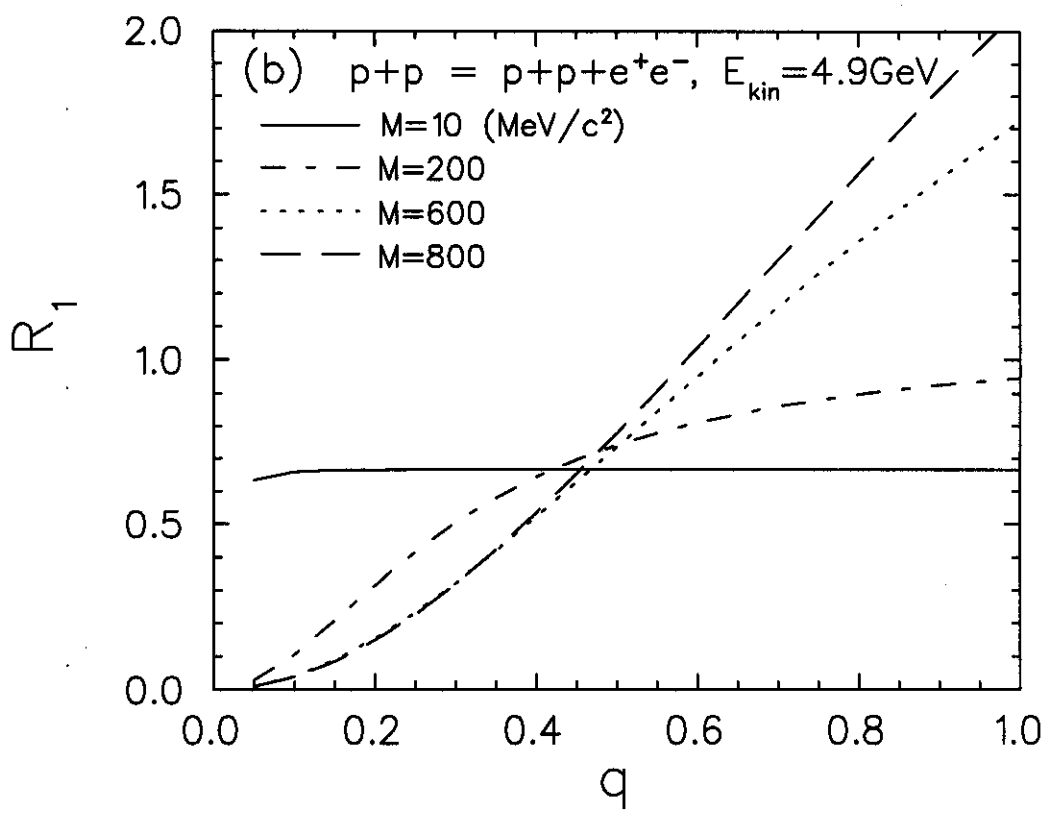
(b) p+p = p+p+e+e−, Ekin=4.9GeV
M=10 (MeV/c²)
M=200
M=600
M=800
R1
q
0.0
0.5
1.0
1.5
2.0
0.2
0.4
0.6
0.8

Fig. 3

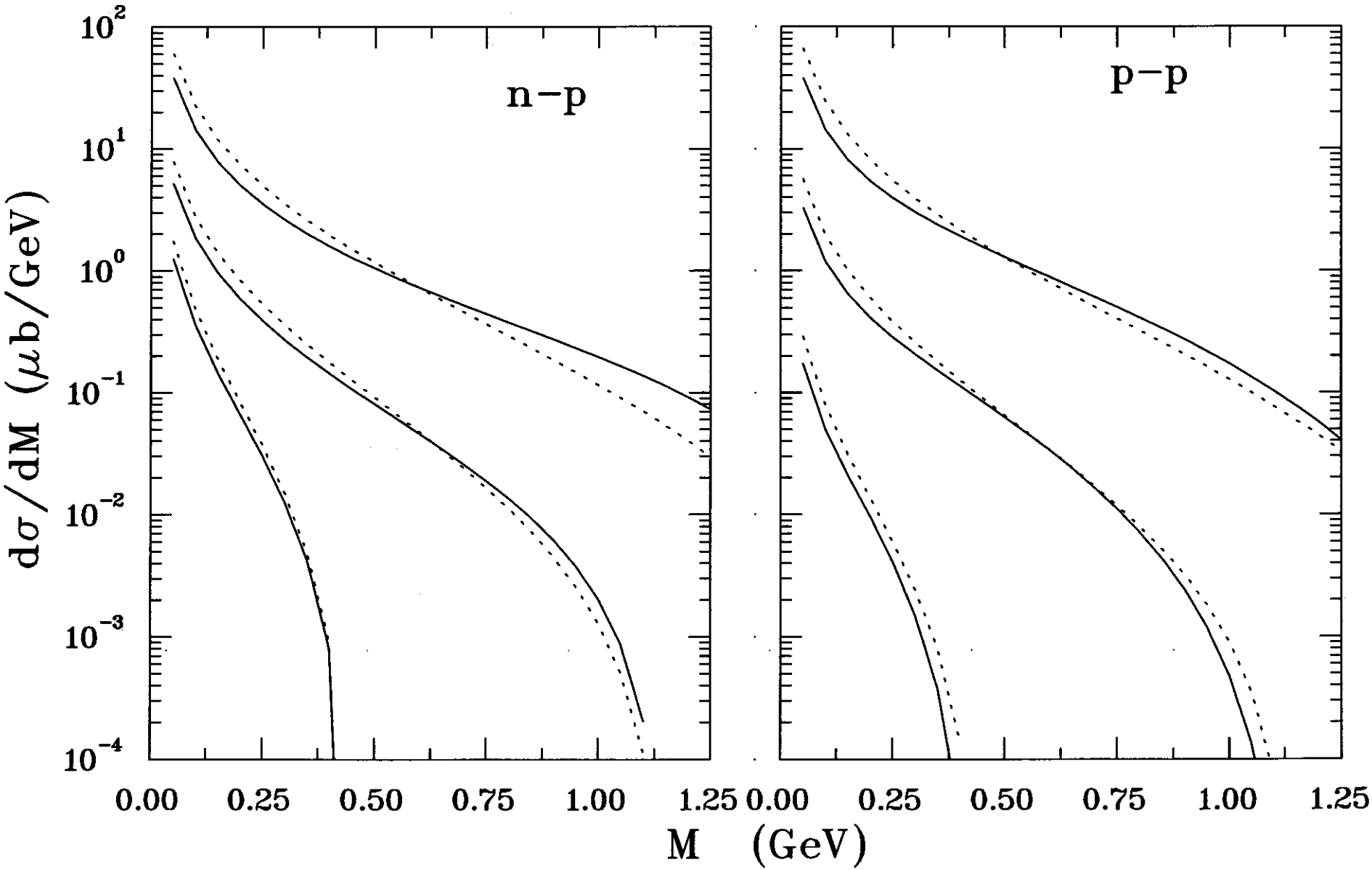
n−p
p−p
dσ/dM (μb/GeV)
M (GeV)
10^2
10^1
10^0
10^-1
10^-2
10^-3
10^-4
0.00
0.25
0.50
0.75
1.00
1.25

Fig. 4

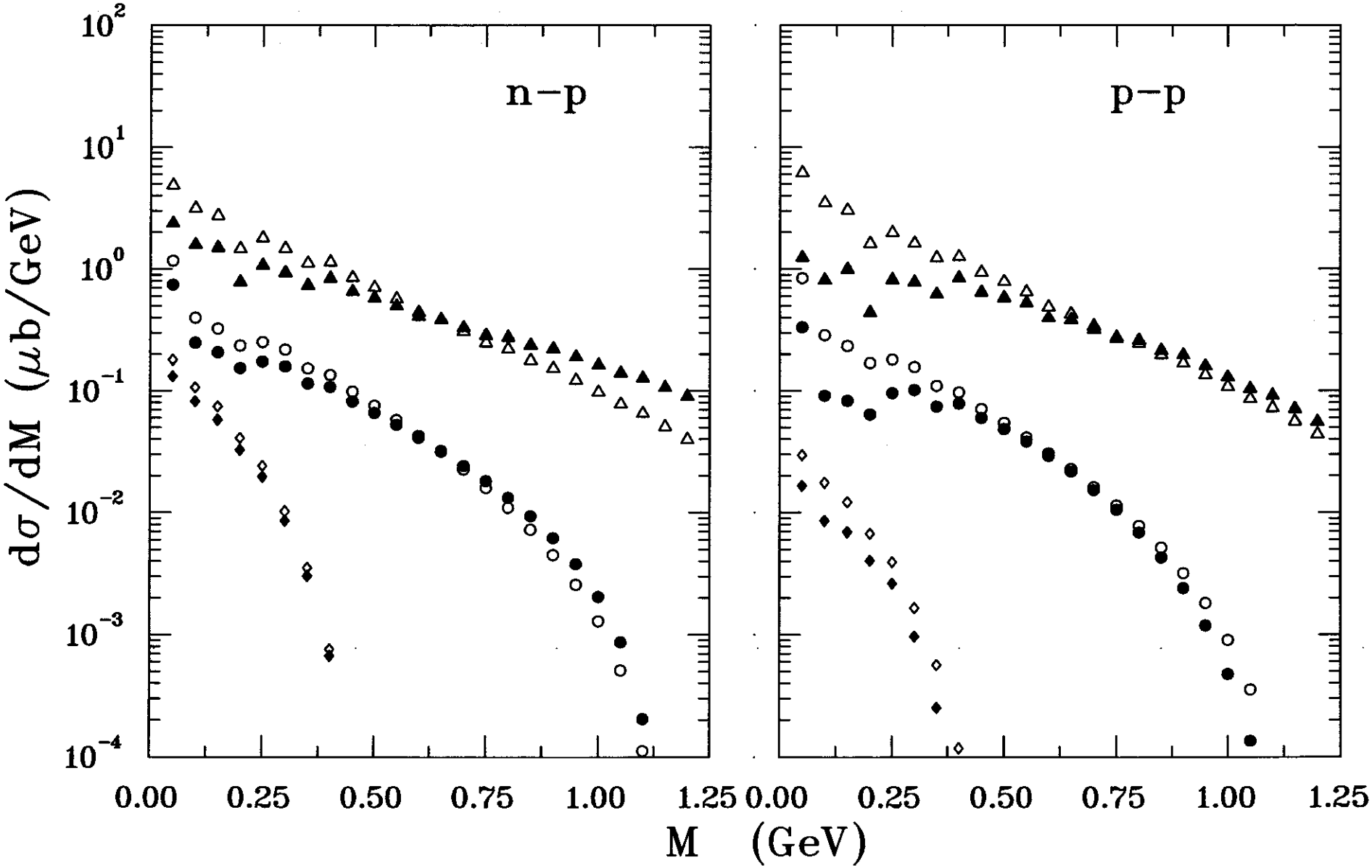
n−p
p−p
dσ/dM (μb/GeV)
M (GeV)
10^2
10^1
10^0
10^-1
10^-2
10^-3
10^-4
0.00
0.25
0.50
0.75
1.00
1.25

Fig. 5

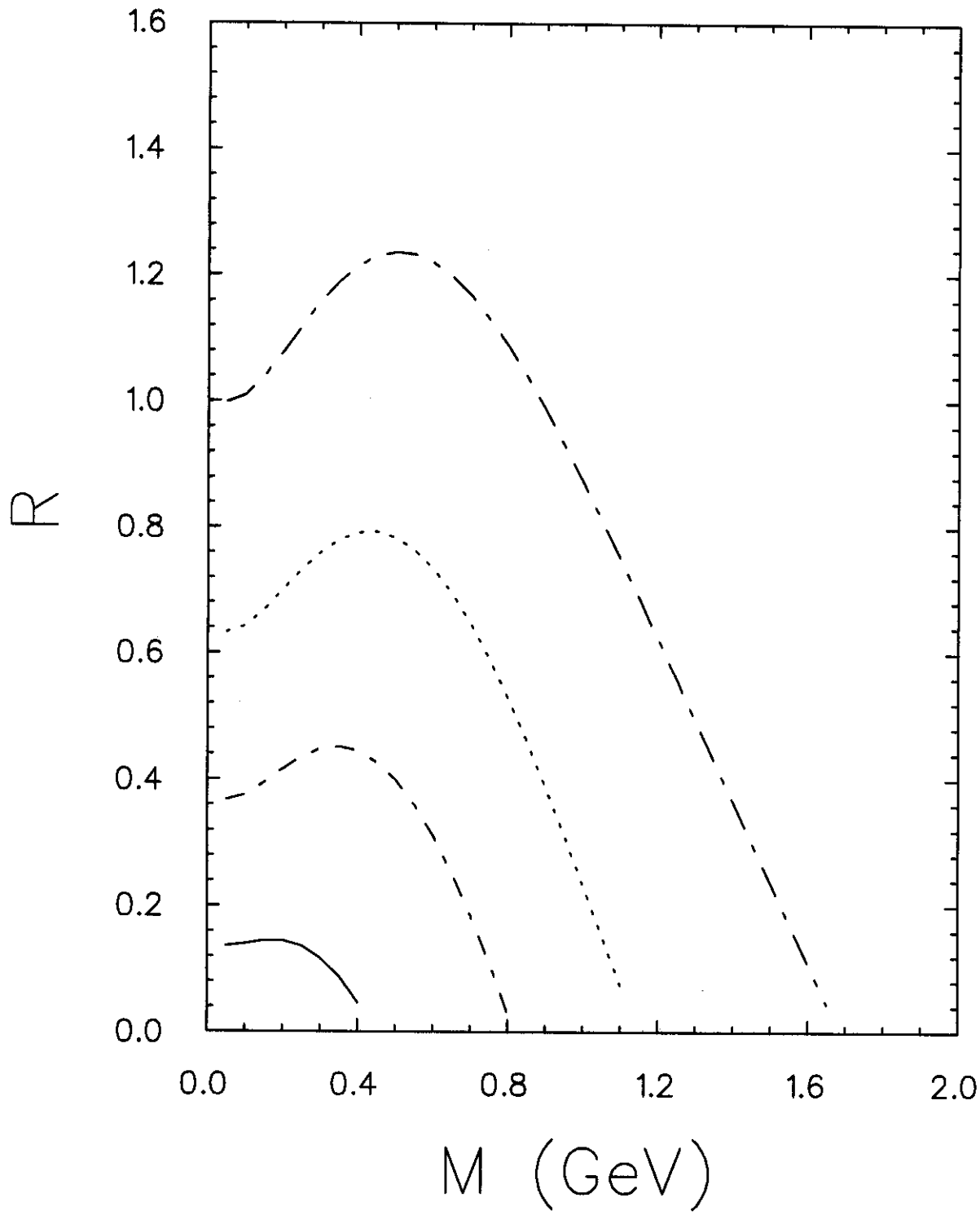

Fig. 6

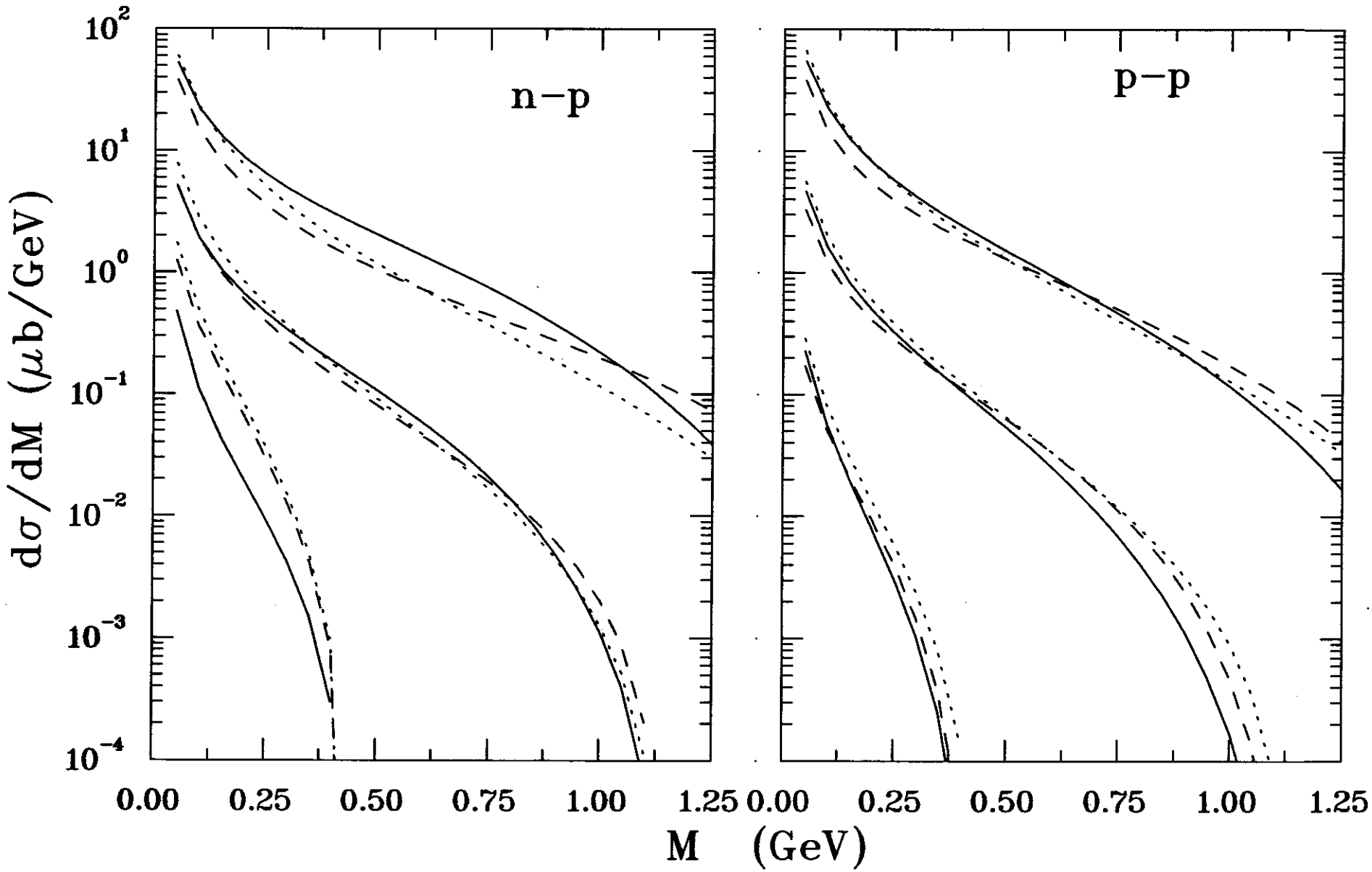
n−p
p−p
dσ/dM (μb/GeV)
M (GeV)
10^2
10^1
10^0
10^-1
10^-2
10^-3
10^-4
0.00
0.25
0.50
0.75
1.00
1.25

Fig. 7

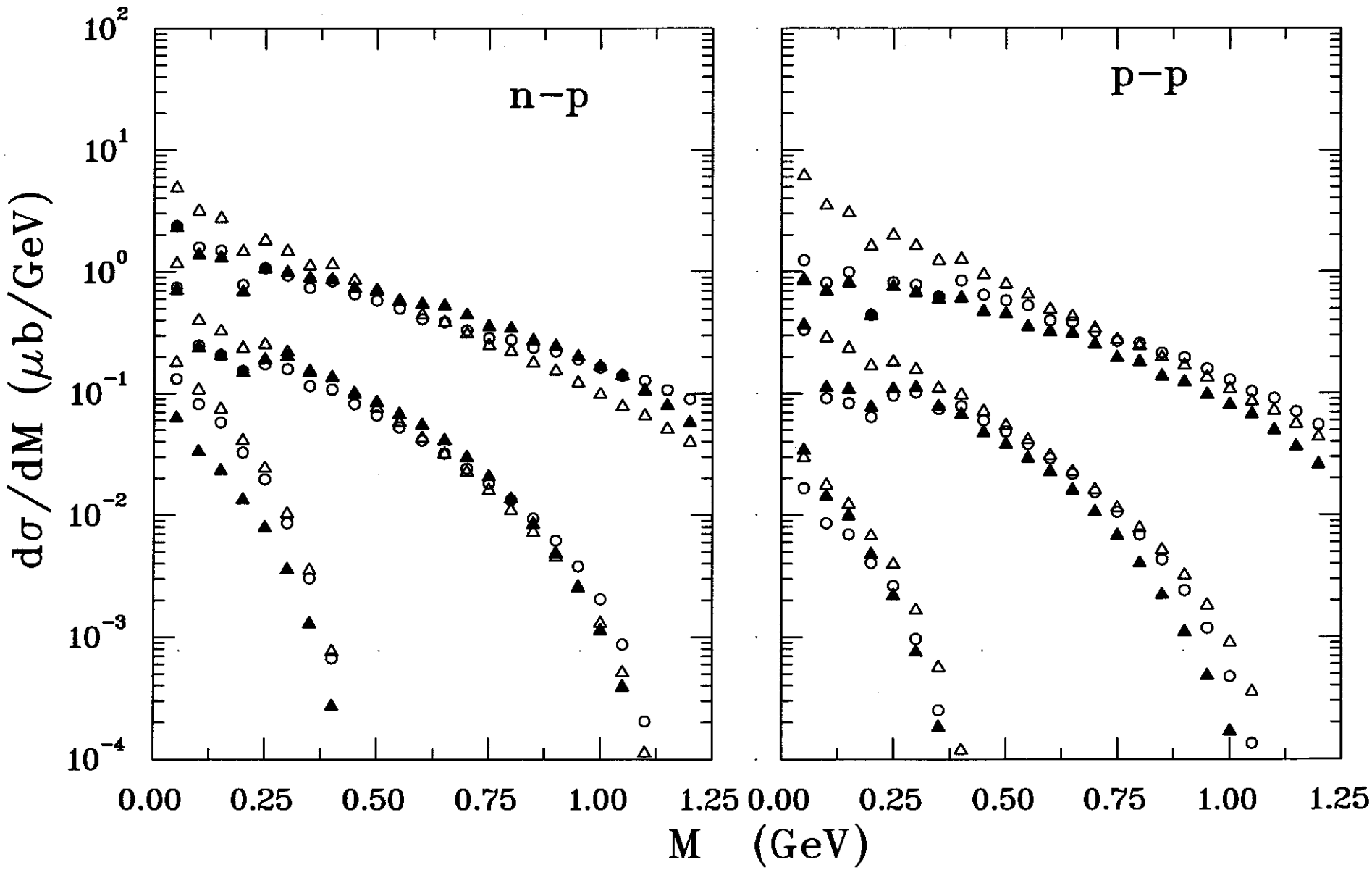
n−p
p−p
dσ/dM (μb/GeV)
M (GeV)
10^2
10^1
10^0
10^-1
10^-2
10^-3
10^-4
0.00
0.25
0.50
0.75
1.00
1.25

Fig. 8

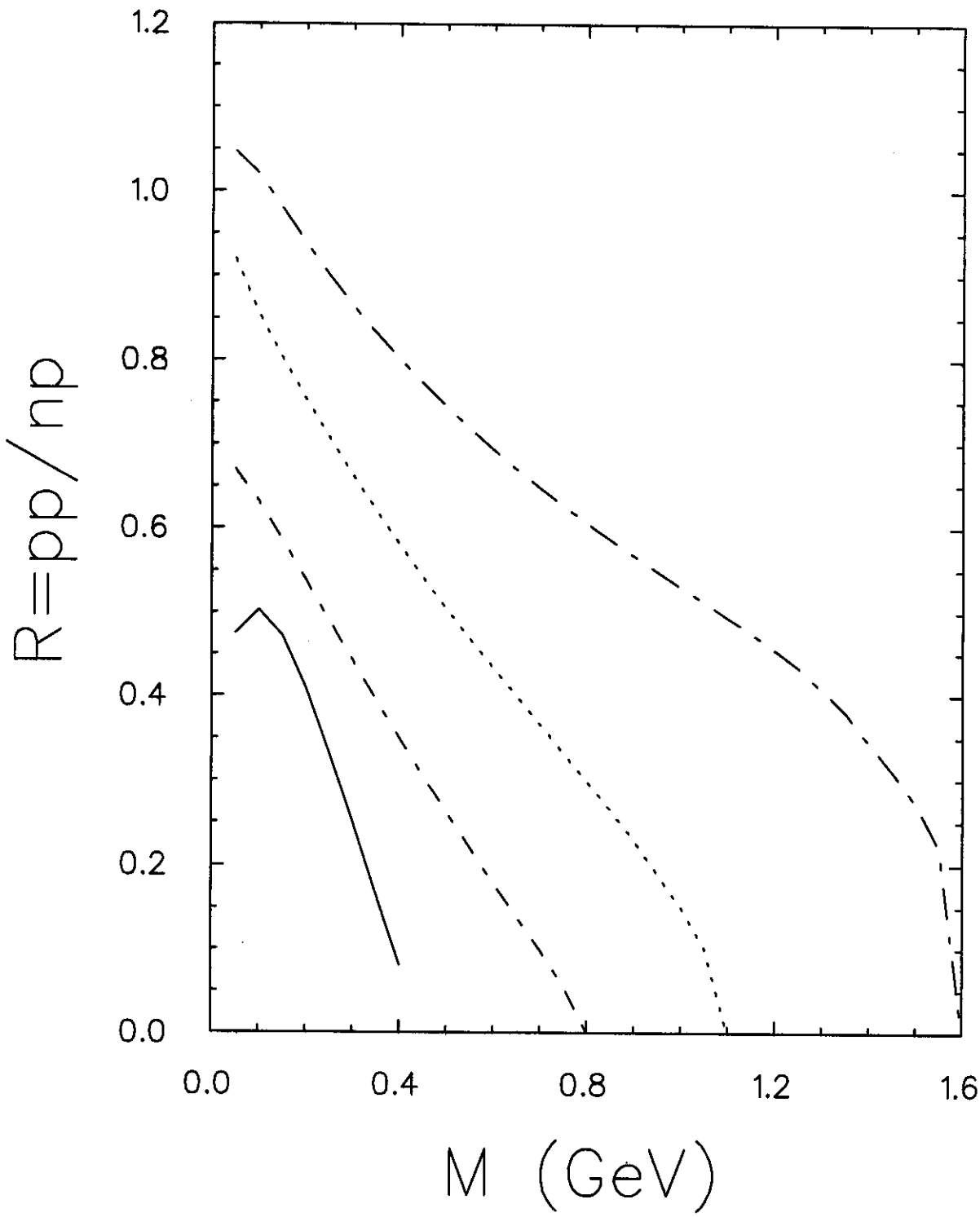

Fig. 9

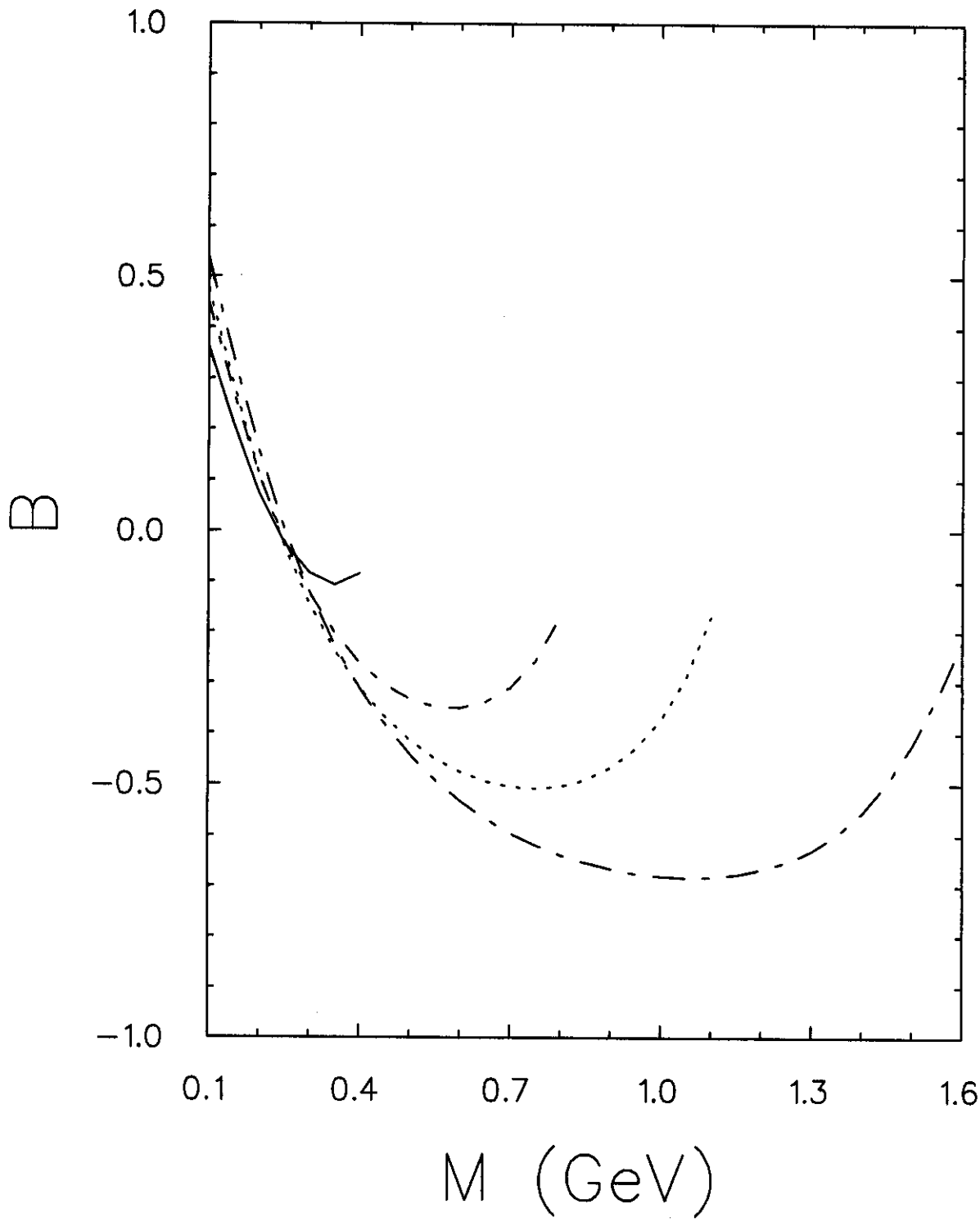

Fig. 10

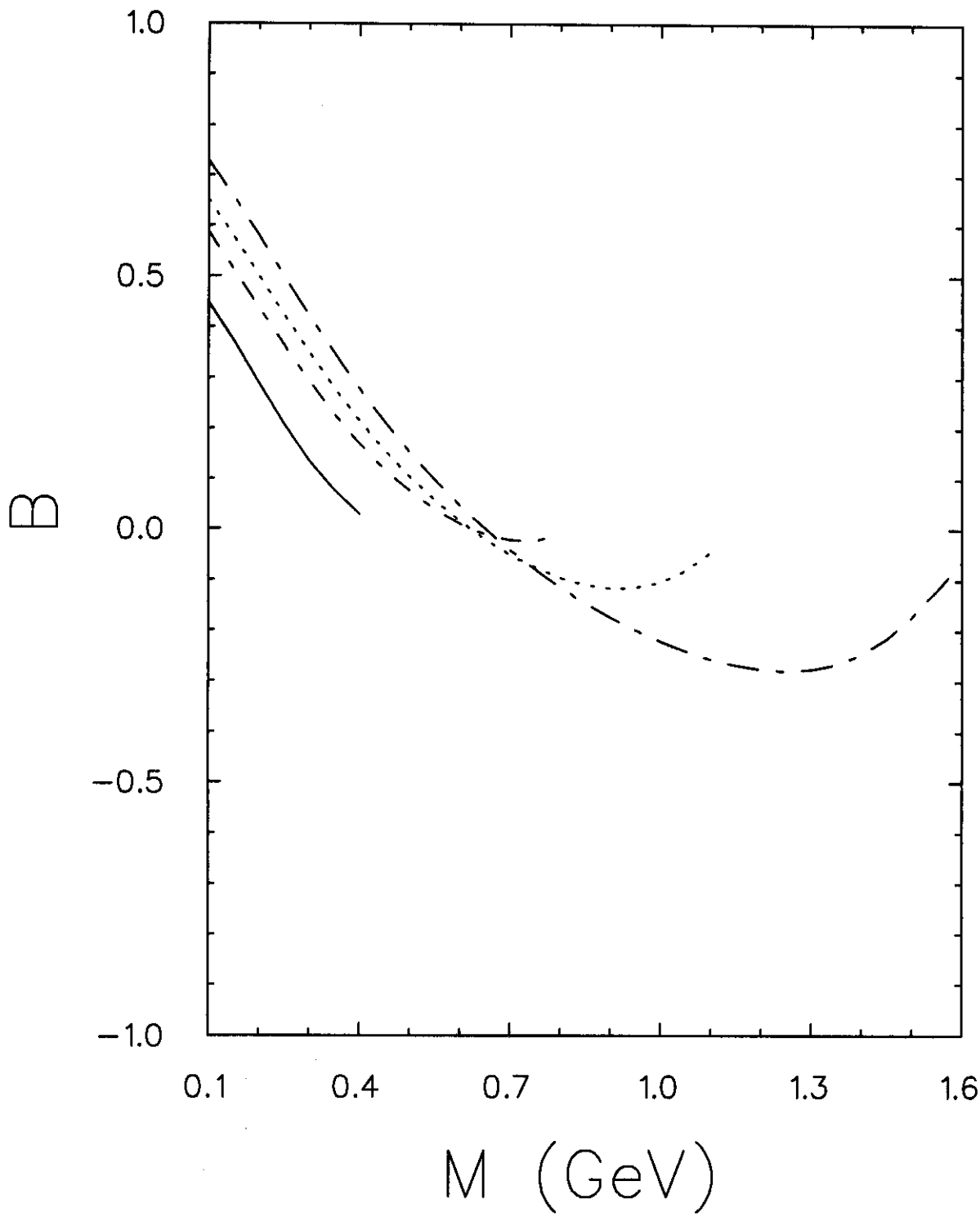

Fig. 11

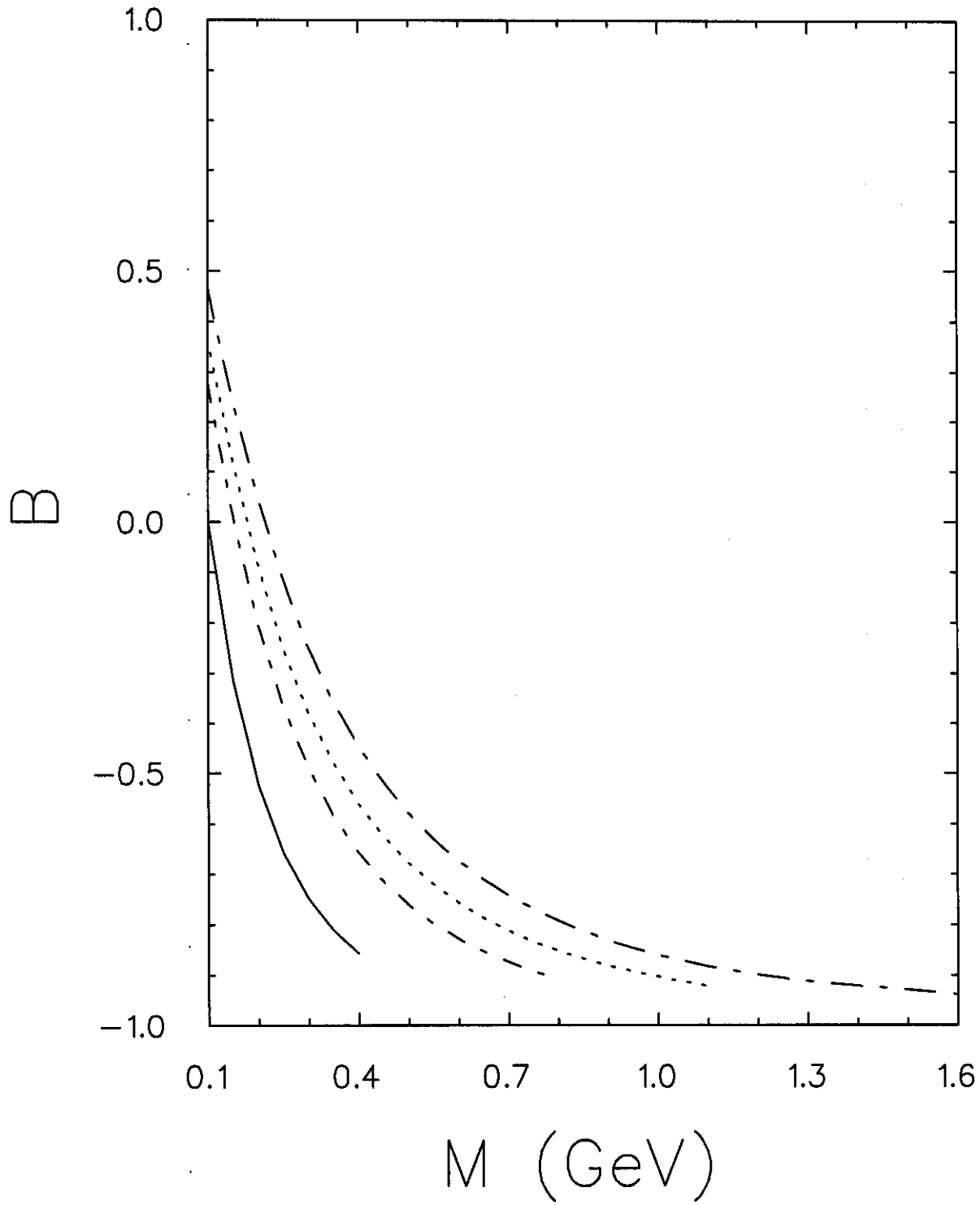

Fig. 12

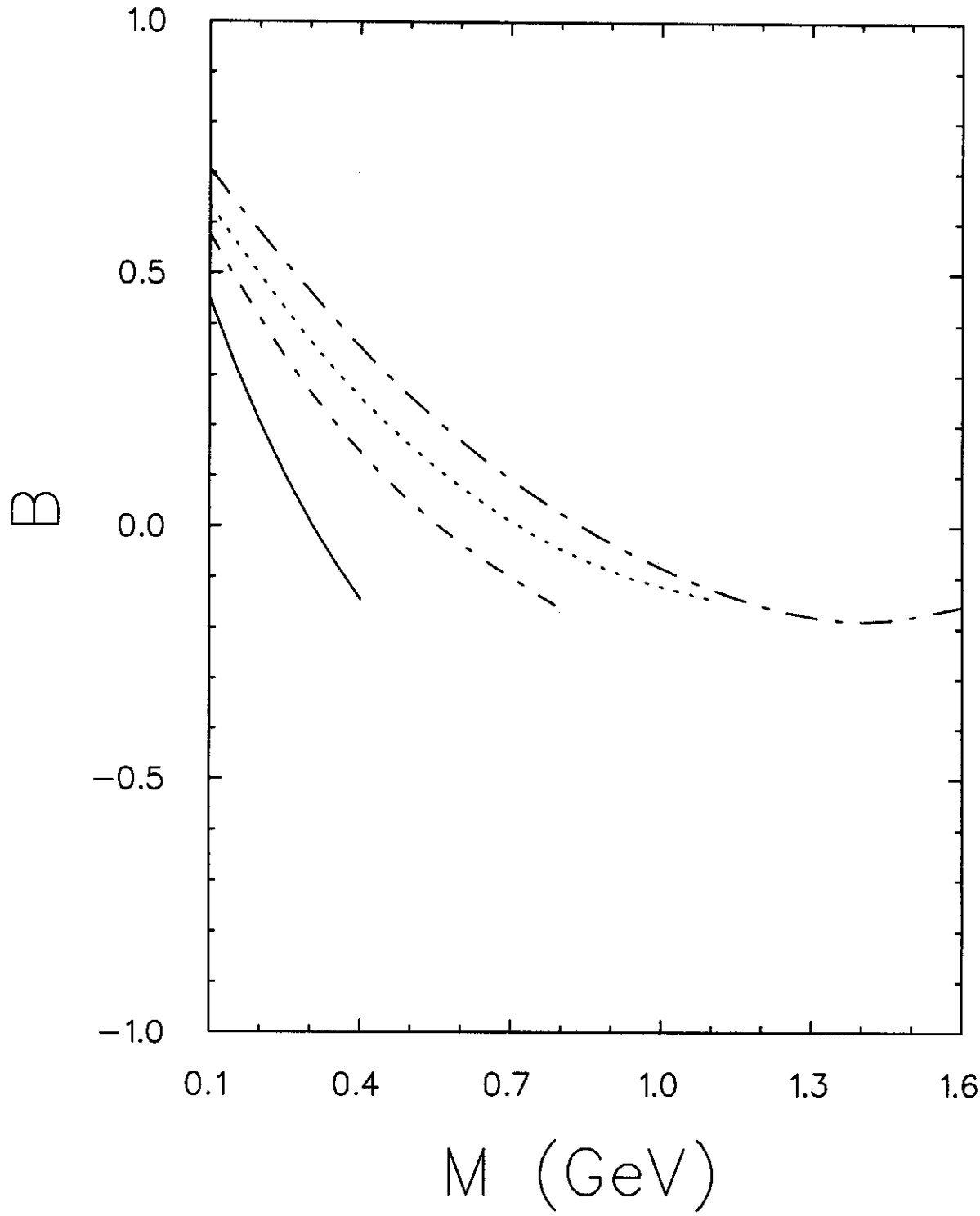

Fig. 13